JJMIE

Volume 17, Number 2, June. 2023
ISSN 1995-6665
Pages 297– 307
https://doi.org/10.59038/jjmie/170213

Jordan Journal of Mechanical and Industrial Engineering

Detecting Technique of COVID-19 Via an Optimized Piezoelectric Sensor

Muath A. Bani-Hani[1*], Mohamed A. Al-Moghazy[2], Wael A. Altabey[2,3],

Sallam. A. Kouritem[2], Mohamed Hakam[4]

[1] Department of Aeronautical Engineering, Jordan University of Science and Technology, Irbid, Jordan.
[2] Department Mechanical Engineering, Alexandria University, Alexandria, Egypt.
[3] International Institute for Urban Systems Engineering, Southeast University, Nanjing, Jiangsu (210096), China.
[4] Department of Textile, Alexandria University, Alexandria, Egypt.

Received 15 Dec 2022 *Accepted 19 Mar 2023*

Abstract

In the last few years, SARS-CoVID-19 pandemic was the main cause of millions of deaths around the world and was the main reason for global economic recession. It is vital to explore noninvasive procedures to detect and eliminate this pandemic expeditious. In this research, we introduce a technique for detecting and quarantine the SARS-CoVID-19 by designing a piezoelectric device with a natural frequency that is equal to the virus structural natural frequency. Because of the resonance effect, the vibration of the device increases, and the power output produced by the piezoelectric layer in the harvester is used to detect the COVID-19 by powering a small LED. The light of the LED is a sign of infection. Furthermore, when the virus's natural frequency is determined, an ultrasonic resonance device can be used to eliminate the virus. Polymerase chain reaction test (PCR) is costly and time-consuming. Our proposed technique is both fast and inexpensive. The installing of the device, the modeling, and the treatment potentiality are discussed in this paper. To maximize the output power of the device at the virus natural frequency, three optimization algorithms are performed. It is observed that Bound Optimization by Quadratic approximation (BOBYQA) optimization algorithm enhances the output power. The analytical model of the proposed sensing device is derived based on the theory of Euler–Bernoulli. The voltage and power frequency response for open and closed circuits are analytically derived. A Finite Element Method (FEM) for the proposed sensing device is developed and analytically verified.

Keywords: 2019-nCoV, piezoelectric, Vibration, Optimization, FEM, COMSOL Multiphysics® software.

1. Introduction

Yao and Wang [1] modeled COVID-19 virus and its spike protein natural frequency in blood. They used FEM to study the modal characteristics of the COVID-19 virus. They founded that the frequencies of the first modes of COVID-19 were very close to each other (198,340,000 Hz), and were 1st bending vibrations. The 3D model and mode shape of 2019-nCoV presented by Yao and Wang [1] are shown in Figure 1. On January 7th, the Chinese government department identified a new coronavirus (2019-nCoV) as the virus that is responsible for a group of pneumonia cases discovered in Wuhan city [2]. As a result of this discovery, the virus has been promptly diagnosed [3, 4]. From the start of COVID-19 until 22 September 2021, this pandemic has infected almost 330 million people of which almost 5 million passed away [5]. Additionally, medical researchers worldwide were making efforts to create vaccines, however, the efficacy of vaccines can diminish if the ribonucleic acid (RNA) of this virus mutates. Although that more than 5,776 million vaccines have been supplied, in many cases the diseases were a global pandemic. A list of COVID-19 tests was introduced that takes several days to obtain result and they are very costly [6]. Time consuming Covid-19 tests can delay detecting the virus and accelerates the infection. This confirms the importance of developing a new technique of testing. Williams and Yates [7] discovered that a mechanical vibration can be transformed to electric charges using piezoelectric materials which couples the electrical and mechanical properties. The surface of a piezoelectric material can experience mechanical strain when subjected to stress, which the material is capable of transforming into an electrical charge (voltage) [8-13]. Khaled et al. [14] optimized the harvester shape employing COMSOL module BOBYQA to reach the maximum output electrical power. Fang et al. [15] presented a reversed PZT beam at different rotational diameters to broadband energy harvester applications. Jian et al. [16] showed a technique for reducing vibrations across a broad range by utilizing a graded PZT beam. Wang et al. [17] suggested a method to widen the operating natural frequency of a PZT harvester, while Li et

* Corresponding author e-mail: Mabanihani@just.edu.jo.

al. [18] studied a structural PZT harvester with both horizontal and vertical installation configurations. Staaf et al. [19] enhanced the bandwidth of their harvester by self-tuning through irregular planning and the inclusion of an additional sliding mass. Rui et al. [20, 21] developed a passive self-tuning piezoelectric energy harvester capable of wideband applications, accomplished through centrifugal force in the rotational structure. Kouritem [22] examined the impact of the 2nd mode of the vibrations of a PZT harvester array, as well as the effects of different materials. Masara et al. [23] devised a method for wideband energy harvesting with an operating frequency of about 10 to15 Hz, featuring a cantilever beam with two parallel gaps. Silveira et al. [24] proposed a harvester for tilting pad journal bearings, highlighting the effect of higher vibrational modes. Finally, Liu et al. [25] showed a broadband natural frequency approach by utilizing four springs (tri-stable mechanism).

Over the last years, remarkable improvements in implantable medical electronics (IMEs) have increased. This can enhance and improve the human life quality. In these days, IMEs such micro–Piezoelectric energy harvesters (PEH) can be utilized as diagnostic and treatment instruments in several human body's regions, such as sensors, cardioverter defibrillators, cardiac pacemakers, and stimulators for the brain, nerves, and bones [26-33]. Previously, research on coronaviruses was primarily focused on their effects on animals. However, there have been several previous outbreaks of coronaviruses in humans, including the severe acute respiratory syndrome (SARS) outbreak in 2002 and the Middle East respiratory syndrome (MERS) outbreak in 2012. Past research was mainly limited on the detection of corona viruses. These limitations were due to many factors including but not limited to: 1-Limited knowledge of the virus. Before the emergence of SARS-CoV-2 there was limited knowledge about the genetic makeup and structure of coronaviruses which made it difficult to develop accurate diagnostic tests [34]. 2-Lack of investment in research. Funding for coronavirus research was limited, as these viruses were not considered a major public health threat until the recent outbreaks [35]. 3-Lack of standardized diagnostic tests. There was no standardized diagnostic test for coronaviruses, which made it challenging for other studies comparison [36]. 4-Limited access to samples. Researchers had limited access to samples of coronaviruses, which made it difficult to study the virus in detail. [37]. 5-Limited availability of advanced technology. Advanced technologies, such as next-generation sequencing and high-throughput screening, were not widely available during previous coronavirus outbreaks, which limited the ability to identify and study the virus [38]. However, there is major development of new technologies to improve the ability to detect and respond to future outbreaks.

In this paper, COVID-19 is modeled using FEM (COMSOL software) as indicated in Figure 2, and analytically based on Euler Bernoulli assumptions of a thin beam. The natural frequencies are close to the ones calculated by Yao and Wang [1].

The proposed piezoelectric sensing device that composes of a cantilever bam is optimized using three different optimization algorithms to resonate with the natural frequency of the COVID-19 protein and to maximize the output electric power. At the resonance, the output power is maximized which is considered as a strong sign of an infection. Then, using the resonance effect or through an ultrasonic device, the virus can be eliminated. The frequency domain voltage and power frequency response functions are presented in this paper as well.

The modeling, installing of the device, and the potential treatment are discussed as well. The validation of proposed FEM COMSOL model is introduced for more confidence in our proposed technique. The natural frequencies evaluated by the finite element model converge with the ones evaluated by Yao and Wang [1]. Figure 3 (b) reveals the proposed technique of detection of COVID-19 in this paper.

2. Installing the proposed piezoelectric sensing device in human body

This section reveals the possibility of using piezoelectric MEMS for detecting and eliminating Covid-19 virus. Ali et al. [39] mentioned the ability to use micro-scale piezoelectric energy harvesters for many biomedical applications. Likewise, by referring to the presented sensitive medical applications of micro-scale piezoelectric sensing device in Figure, we are proposing a micro-scale sized and high-frequency piezoelectric energy harvester/sensor to detect and weaken the virus. Figure 3(b) shows the device with a frequency equals to the natural frequency of COVID-19 to achieve resonance. This is the first step in the design to detect the virus spike protein structures. The motion of the spike can be considered as base excitation for the proposed device

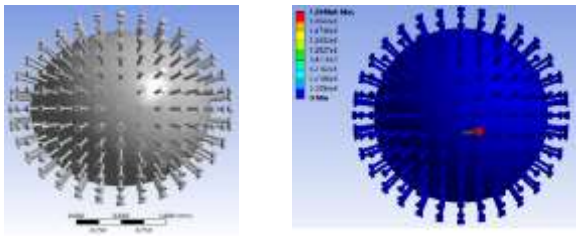

(a) (b)

Figure 1. (a) 3D model of 2019-nCoV, (b) Mode shape of the tuned 2019-nCoV model [1].

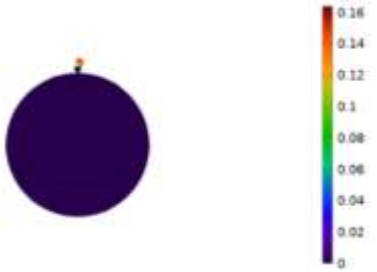

Figure 2. Mode shape of single spike protein obtained using FEM COMSOL.

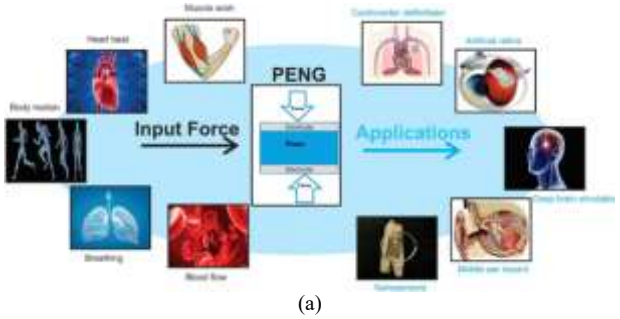

(a)

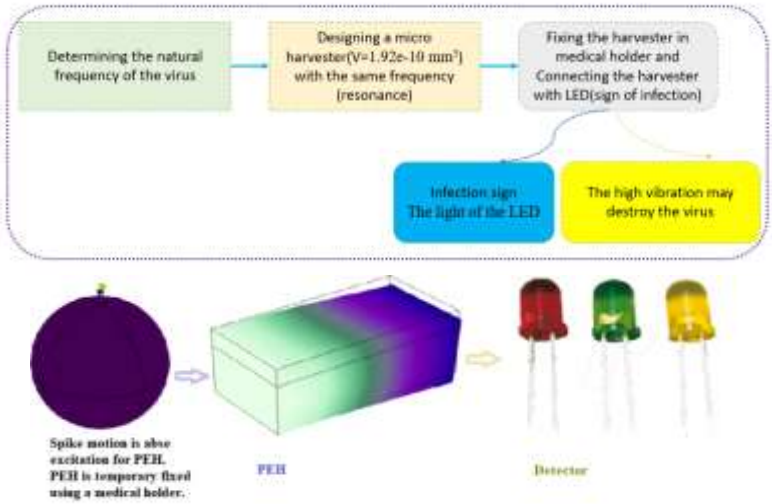

(b)

Figure 3. (a) use the micro scale piezoelectric energy harvester (PEH) in biomedical applications [9], (b) our proposed micro scale piezoelectric sensing device for detecting and eliminating the COVID-19

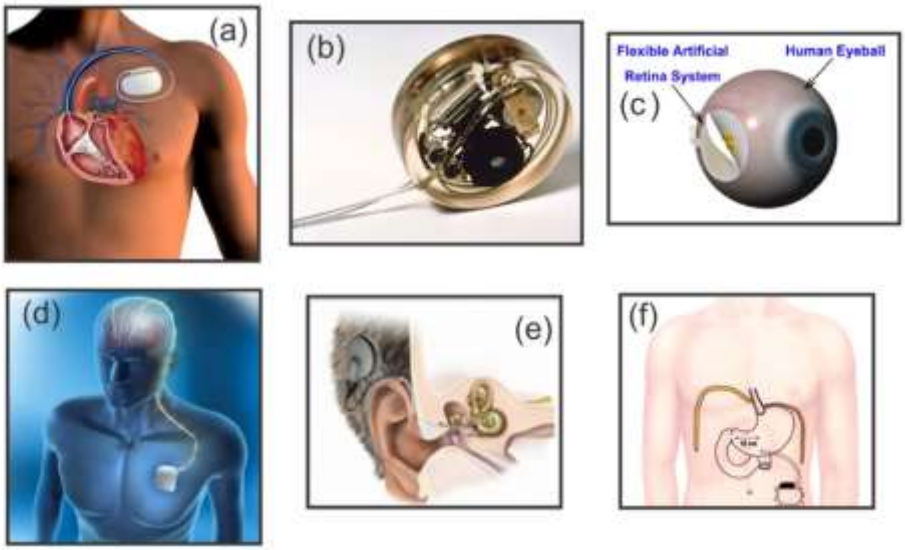

Figure 4. (a) Implantable cardioverter defibrillators (by Washington Heart Rhythm Associates, LLC). (b) Siemens's cardiac pace makers (c) Artificial retina system implanted in a human eye [20], and (d) Deep brain stimulation (by Epilepsy Society), (e) Middle ear implant (by Sp Hear Clinic), and (f) Gastric stimulator implanted in body [26].

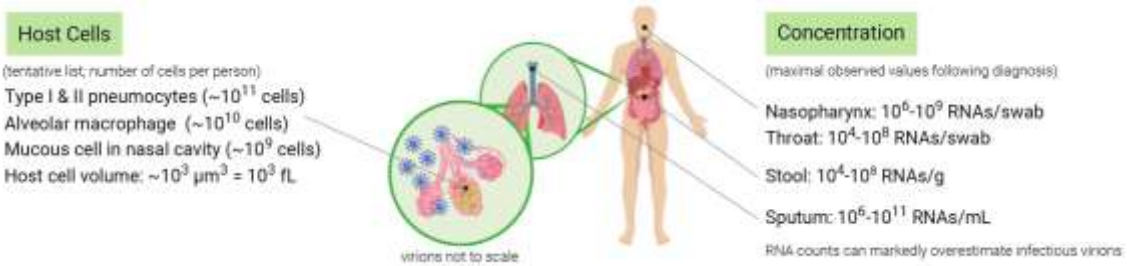

Figure 5. Concentration of the COVID-19 in the infected body [30]

The value of this excitation is $3.5x10^{-12}$ m [1]. Once the virus is detected, it can be eliminated using an ultrasonic resonance device.

In recent decades, significant progress in microelectronics, has led to the advancement in developing various implantable medical electronics (IMEs) that utilize micro-scale piezoelectric energy harvesters. These days, IMEs can be inserted into different soft tissues of the human body such as cardioverter defibrillators, sensors, cochlear implants, cardiac pacemakers, artificial retinas, and stimulators for nerves, brains, and bones[26-33]. (See Figure 4). These implantable devices can provide diagnostic information, such as monitoring temperature, blood pressure, and heart rate for various diseases while simultaneously supporting treatments, such as stimulating the brain and muscles. For instance, a typical pacemaker can play a supportive role in adjusting irregular heartbeats due heart blockage, for example. Therefore, it is proposed to use the microscale harvester as thoracoscopy, for example, to help chest doctors to exhibit fast and high-quality treatment. In theory, it is possible to weaken or deactivate the 2019-nCoV virus by disrupting the virus's spike protein using resonance, which could aid the immune system in clearing the virus from the body. Figure 5 indicates the concentration of the COVID-19 in human body [40]. This concentration is utilized to determine the places in human body where the proposed micro-scale piezoelectric sensing device can be used. Finally, Cho et al. [41]proved the possibility to fix a piezoelectric energy sensing device in a moving human part similar to what it is proposed in this work. They also optimized a harvester to operate a LED indicator to measure strain, temperature, and leakage value in real time.

3. Modeling of the sensing device

3.1. Modeling Using FEM

This paper introduces a potential solution based on resonance phenomena to detect and eliminate 2019-nCoV. The structure of CoV-19 comprises a spherical virus with spike proteins located on its surface. When the 2019-nCoV virus infects a person, it attaches its spike proteins to receptors on the cell membrane, allowing it to enter and replicate within the host's cells. Yao and Wang [1] evaluated the natural frequency and vibration amplitude of the spike protein. Therefore, the virus can be detected at early stages and this may save time, effort, and cost through designing a micro-scale piezoelectric energy device that resonates with COVID-19 virus natural frequency.

The frequency of the COVID-19 can be considered as an ultrasonic vibration source (198,340,000 Hz) and small vibration amplitude. The piezoelectric layer on the proposed device can convert the vibration into electrical power. The harvested electrical power can operate led power (assign of infection or detection process). The modeling of the piezoelectric device and analysis are performed using finite element analysis (FEM) COMSOL. Figure 5 shows the dimensional and proposed piezoelectric sensing device model. Several attempts using an iterative optimization are conducted to reach the targeted natural frequency of the COVID-19. In the next section, the optimization COMSOL module is utilized to model a piezoelectric energy device with frequency equals the virus frequency and with a maximum output power. The micro-scale device consists of a copper base layer with dimensions of $10x10^{-4}$ mm × $5x10^{-4}$ mm × $2.85x10^{-4}$ mm[42]. The base layer is covered with a piezoelectric layer of PZT-5H with dimensions of $10x10^{-4}$ mm × $5x10^{-4}$ mm × $1x10^{-4}$ mm. The total volume of the micro-scale device is $1.92x10^{-10}mm^3$. Copper has a density and a modulus of elasticity of 8,940 kg/m^3 and126 GPa, respectively. The piezoelectric material has a density and a modulus of elasticity of 7500 kg/m^3 and 71 GPa, respectively. Figure 6reveals the FE meshing distribution of the proposed model. Figure 7indicates the 1stmode shape and natural frequency of the proposed model.

In Figure 6, the piezoelectric layer is assumed to be attached and glued to the copper layer with a very thin epoxy adhesive. The epoxy effect can be neglected due its very low elasticity, density and weight. However, in the FEM simulation of the proposed sensing device, the copper and piezoelectric layers' interaction and the epoxy adhesive are all taken into consideration to accurately simulate the model and obtain accurate results when modeling, developing and simulating the proposed device using COMSOL FEM software.

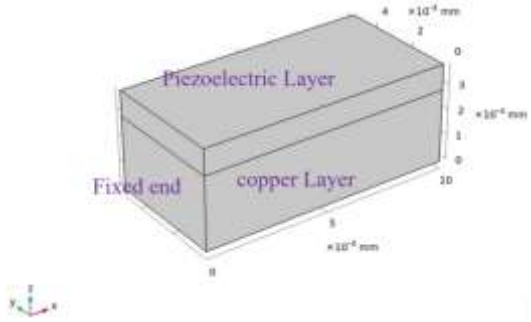

Figure 5. The dimensional piezoelectric proposed sensing device

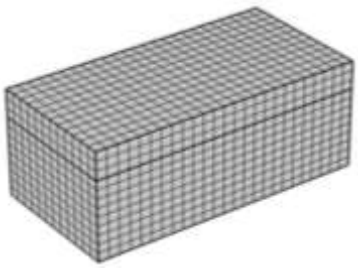

Figure 6. The model FEM meshing

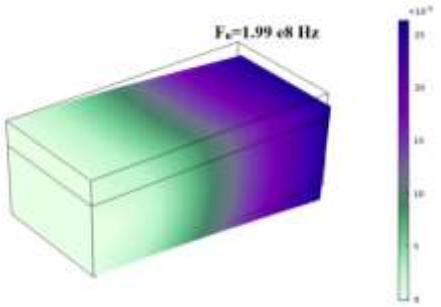

Figure 7. The harvester natural frequency.

3.2. Analytical Modelling

The analytical model of the corresponding cantilever beam indicated in Figure 6can be derived per the assumptions of Euler–Bernoulli theory[43, 44]. The governing equation of the relative deflection of the beam with respect to its base deflection can be expressed as in[45].

$$m\frac{\partial^2 w_{rel}}{\partial t^2} + c\frac{\partial w_{rel}}{\partial t} + YI\frac{\partial^4 w_{rel}}{\partial x^4} + \vartheta\left[\frac{d\delta(x)}{dx} - \frac{d\delta(x-L)}{dx}\right]V(t) = -m\frac{\partial^2 w_b}{\partial t^2} \quad (1)$$

$w_{rel}(x,t)$ is the deflection. The base is denoted by $w_b(x,t)$. The damping coefficient is denoted by c. The beam bending stiffness is denoted by YI. $\delta(x)$ is the delta function.$m$is expressed and indicated in (2) that represents the mass per length of the device.ϑ is the coupling coefficient.

$$m = b(\rho_s h_s + 2\rho_p h_p) \quad (2)$$

Using the standard modal analysis and the PZT constitutive relation [46], the modal response of the composite beam of the proposed sensing device can be obtained as indicated in (3) and (4)[47].

$$\ddot{T}(t) + 2\xi\omega_n\dot{T}(t) + \omega_n^2 T(t) + \alpha V(t) = f(t) \quad (3)$$

$$C_p\dot{V}(t) + \frac{V(t)}{R_l} = \alpha\dot{T}(t) \quad (4)$$

Where $T(t)$ represents the temporal function of the beam relative deflection. ξ is the damping ratio. ω is the natural frequency. α is the modal coupling coefficient.$f(t)$ is the modal mechanical forcing function due to the beam base excitation. C_p is the capacitance of the composite beam.$V(t)$ is the voltage difference through the electric resistance denoted by R_l.

It must be noted that sometimes it is more convenient to represent the electromechanical differential equation (3)according to energy harvesting circuitry-based literature[48, 49]. Therefore, the PZT layer can be represented as a dependent current source$i_p(t)$that are connected in parallel with its internal capacitanceC_p[50]as illustrated in Figure 8.

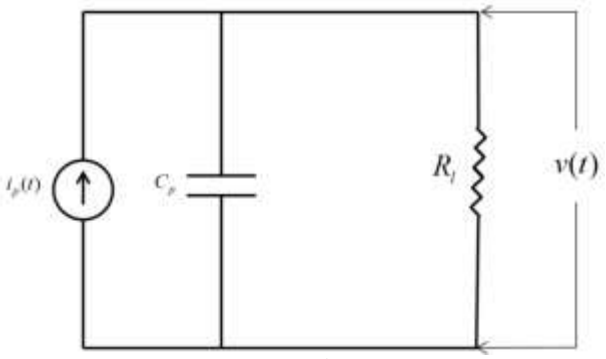

Figure 8. Electrical circuit of the piezoelectric beam

The fundamental/resonance frequency ω_n of the 1st vibration mode obtained analytically is equal to $1.992\ x\ 10^8\ Hz$which is very close the 1st natural frequency obtained numerically in Figure 8. At this point, the frequency domain voltage and power frequency response functions can be represented by using Laplace and then Fourier transform as indicated in (5).

$$Voltage\ FRF = \frac{V(\omega)}{F(\omega)} = \frac{\frac{j\omega\ \alpha}{2j\omega\ \xi\ \omega_n\ + (\omega_n^2 - \omega^2)}}{(C_p\ j\omega + \frac{1}{R_l}) + \frac{j\omega\ \alpha^2}{2j\omega\ \xi\ \omega_n\ + (\omega_n^2 - \omega^2)}} \quad (5)$$

The power frequency response function (FRF) can be expressed simply as indicated in (6).

$$Power\ FRF = \frac{1}{R_l}\left[\frac{V(\omega)}{F(\omega)}\right]^2 \quad (6)$$

The analytical voltage and power functions are obtained against a wide range of excitation frequencies as will be discussed in section 5.1. From the frequency response functions, two excitation frequencies of the 1st vibrational mode are obtained. These frequencies are referred to as the short and open circuit resonance frequencies that are denoted by ω_{SC} and ω_{OC}, respectively. Their values are approximately equal to $1.995\ x\ 10^8\ Hz$ and $2.06\ x\ 10^8\ Hz$, respectively according to[1].

4. Optimization of the Proposed Device

Several optimizations techniques are utilized in this section to maximize the output power [51-54].A Generalized Normal Distribution Optimization (GNDO) algorithm is employed to optimize the proposed piezoelectric device structure with additional constrains on the frequency [55].Iterative techniques have been employed extensively for optimizing power systems in various applications [14, 56, 57].

In this study, the optimization is worked out using the COMSOL optimization module using a BOBYQA solver. A BOBYQA is an optimization algorithm used to optimize a cost function, where each iteration uses a quadratic approximation [58]. Furthermore, a COBYLA optimization method is employed in this study. COBYLA optimization algorithm is a numerical optimization technique that can be used for constrained optimization problems [59].Nelder–Mead optimization technique is also employed in this study. Nelder–Meadmethod is a technique is utilized to get the maximum or minimum of a fitness function. The Nelder–Mead optimization algorithm can be denoted as a heuristic search technique that can converge to non-stationary points[59].

The optimization tool using COMSOL module is set with tolerance of the penalty factor parameter equals to 0.5, multiplication factor of the penalty factor is set at10, upper bound of Lagrange multiplier is1.79, constrain tolerance equals to 0.01, and the maximum iterations are set at1000.Figure 9graphically describes the general steps of the BOBYQA optimization technique. More details of the three optimization methods can be obtained from the cited references.

The optimization is performed to maximize the generated power. The optimizable parameters include the harvester length (L), the harvester width (W), base material thickness (t_s), and the piezoelectric thickness (t_p). Furthermore, the natural frequency of the proposed sensing device is constrained as to match the virus's natural frequency.

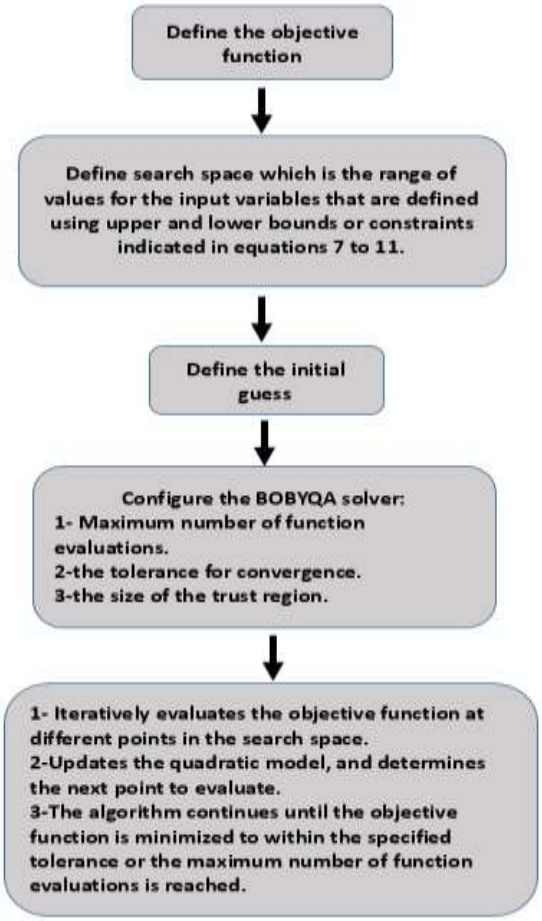

Figure 9. Flow chart of the optimization technique.

The optimization problem can be expressed as the following:

Maximize: Total kinetic energy subject to:

$$10x10^{-4}\ mm \leq L \leq 15x10^{-4}\ mm \quad (7)$$

$$5\ x10^{-4}mm \leq W \leq 6\ x10^{-4}mm \quad (8)$$

$$1.5\ x10^{-4}\ mm \leq ts \leq 3.2\ x10^{-4}\ mm \quad (9)$$

$$1x10^{-4}mm \leq t_p \leq 3x10^{-4}mm \quad (10)$$

$$\omega_n = 1.99\ x\ 10^{8}Hz \quad (11)$$

The natural frequency (ω_n) is indicated in the optimization process as an quality constraint to match the virus natural frequency. Table 1 reveals the results of the optimization process indicating the upper and lower values of the optimizable parameters. The fixed values of parameters constraints depend on the design parameters.

The best result is found using the BOBYQA optimization technique. The optimal parameters obtained from the optimization are $L = 10\ x10^{-3}mm$, $W = 5.3\ x10^{-3}mm$, $t_p = 1\ x10^{-3}mm$, and $t_s = 2.99\ x10^{-3}mm$.

The BOBYQA optimization technique was utilized, and its selected results are presented in Table 2. The table demonstrates the successful convergence of the optimizable parameters in meeting the virus natural frequency constraint. Additionally, it is evident that the thickness and width of the base material are more influential than the length and thickness of the piezoelectric material that are slightly affecting the frequency and kinetic energy. Table 3reveals some selected results based on COBYLA optimization technique. Table 4reveals some of the results obtained using the Nelder-Mead optimization technique.

Table 1. Upperand lower bounds of the optimized sensing device.

Device parameters	Lower Bound	Upper Bound	Optimum Solution
(L mm)	10e-4	15e-4	10e-3
(wmm)	5e-4	6e-4	5.3 e-4
(t_p mm)	1e-4	3e-4	1e-4
($t_s$mm)	1.54e-4	3.2e-4	2.99e-4

Table 2. BOBYQA optimization technique.

Iteration No.	t_s (m)	t_p (m)	l (m)	w (m)	Objective
1	2.99E-07	1.00E-07	1.00E-06	5.10E-07	6.72E-37
2	2.99E-07	1.00E-07	1.00E-06	5.30E-07	6.91E-37
3	2.99E-07	1.00E-07	1.00E-06	5.20E-07	6.81E-37
4	2.99E-07	1.00E-07	1.00E-06	5.14E-07	6.76E-37
5	2.99E-07	1.04E-07	1.00E-06	5.08E-07	6.35E-37
6	2.97E-07	1.04E-07	1.00E-06	5.12E-07	6.41E-37
7	2.96E-07	1.05E-07	1.00E-06	5.16E-07	6.34E-37
8	2.94E-07	1.03E-07	1.00E-06	5.11E-07	6.41E-37
9	2.99E-07	1.00E-07	1.00E-06	5.12E-07	6.74E-37
10	2.99E-07	1.01E-07	1.00E-06	5.11E-07	6.63E-37
11	2.95E-07	1.06E-07	1.00E-06	5.15E-07	5.92E-37
12	2.99E-07	1.01E-07	1.00E-06	5.09E-07	6.62E-37
13	2.99E-07	1.01E-07	1.00E-06	5.09E-07	6.65E-37
14	2.98E-07	1.02E-07	1.00E-06	5.10E-07	6.55E-37
15	2.99E-07	1.01E-07	1.00E-06	5.08E-07	6.62E-37
16	2.98E-07	1.01E-07	1.00E-06	5.09E-07	6.63E-37
17	2.99E-07	1.00E-07	1.00E-06	5.09E-07	6.67E-37
18	3.00E-07	1.01E-07	1.00E-06	5.09E-07	6.63E-37
19	2.98E-07	1.01E-07	1.00E-06	5.09E-07	6.61E-37
20	2.99E-07	1.02E-07	1.00E-06	5.09E-07	6.53E-37

Table 3. COBYLA optimization technique.

Iteration No.	t_s (m)	t_p(m)	l (m)	w (m)	Objective
1	3.02E-07	1.21E-07	1.01E-06	5.01E-07	4.94E-37
2	2.97E-07	1.02E-07	1.01E-06	5.12E-07	6.59E-37
3	2.93E-07	1.03E-07	1.01E-06	5.09E-07	6.45E-37
4	2.93E-07	1.03E-07	1.01E-06	5.09E-07	6.45E-37
5	2.93E-07	1.03E-07	1.01E-06	5.09E-07	6.45E-37
6	2.93E-07	1.03E-07	1.01E-06	5.09E-07	6.45E-37
7	2.93E-07	1.03E-07	1.01E-06	5.09E-07	6.45E-37
8	2.97E-07	1.02E-07	1.01E-06	5.12E-07	6.59E-37

Table 4. Nelder-Mead optimization technique.

Iteration No.	t_s (m)	t_p (m)	l (m)	w (m)	Objective
1	2.62E-07	1.46E-07	1.00E-06	5.11E-07	3.56E-37
2	2.63E-07	1.45E-07	1.00E-06	5.13E-07	3.60E-37
3	2.62E-07	1.46E-07	1.00E-06	5.13E-07	3.56E-37
4	2.64E-07	1.43E-07	1.00E-06	5.13E-07	3.69E-37
5	2.61E-07	1.48E-07	1.00E-06	5.12E-07	3.49E-37
6	2.61E-07	1.48E-07	1.00E-06	5.12E-07	3.50E-37
7	2.62E-07	1.47E-07	1.00E-06	5.12E-07	3.52E-37
8	2.61E-07	1.48E-07	1.00E-06	5.15E-07	3.49E-37
9	2.62E-07	1.47E-07	1.00E-06	5.12E-07	3.54E-37
10	2.62E-07	1.47E-07	1.00E-06	5.13E-07	3.54E-37
11	2.62E-07	1.47E-07	1.00E-06	5.13E-07	3.52E-37
12	2.61E-07	1.48E-07	1.00E-06	5.14E-07	3.51E-37
13	2.62E-07	1.47E-07	1.00E-06	5.13E-07	3.53E-37
14	2.61E-07	1.48E-07	1.00E-06	5.11E-07	3.47E-37
15	2.62E-07	1.47E-07	1.00E-06	5.13E-07	3.54E-37
16	2.63E-07	1.46E-07	1.00E-06	5.13E-07	3.57E-37
17	2.62E-07	1.48E-07	1.00E-06	5.13E-07	3.51E-37

5. Simulation analysis

5.1. simulation of the analytical solution

This section discusses the voltage and power frequency response functions obtained through analytical methods for

various excitation frequencies, which are depicted in Figure 10(a) and (b). The figure highlights two critical resonance frequencies of the 1st vibration mode, (ω_{SC}) and (ω_{OC}), with values approximately equal to $1.995\ x10^8 Hz$ and $2.06\ x10^8 Hz$, respectively. Additionally, Figure 11, (a) and (b) show, in the frequency domain, the voltage and power frequency response functions that are obtained for different resistive loads particularly at the open circuit 1st natural frequency. It is observed that the voltage increases with increasing load resistance. However, the power reaches its peak at a certain value of the resistive load. Therefore, the optimal resistive load of the un-optimized device at the short and open circuit resonance frequencies where the power reaches its peak, are roughly $1.672\ k\Omega$ and $19.44\ k\Omega$, respectively as they clearly can be indicated in Figure 11 (b).

5.2. Numerical verification

The finite element model (FEM) results of the un-optimized piezoelectric device are analytically verified in this section. The finite element analysis is used to find the 1st natural frequency of the proposed un-optimized sensing device and the results are compared to the ones obtained by the analytical model. Figure (a) and (b)illustrate the voltage and power response functions in the frequency domain by the (FEM) and the analytical models results in terms of the 1st natural frequency, respectively. Table 5 shows a very good matching between the two methods with a maximum $error = 0.1\%$. The voltage and power response functions are at a base excitation of $3.5x10^{-12}$ m, are obtained using the FEM method and compared to the one obtained analytically versus a broad range of excitation frequencies and are indicated in Figure 12respectively.

Table 5. 1st natural frequency comparison of the FE and analytical models.

Analytical	**1.992 x 10^8 Hz**
FEM	1.99 x 10^8 Hz
Error %	0.1

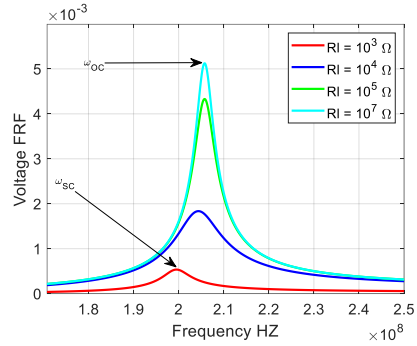

(a)

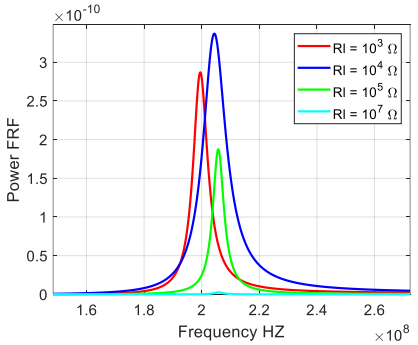

(b)

Figure 10. Frequency response function (a) Voltage (b) Power.

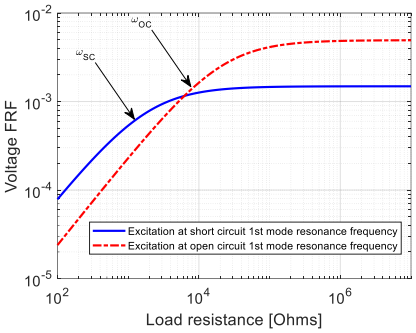

(a)

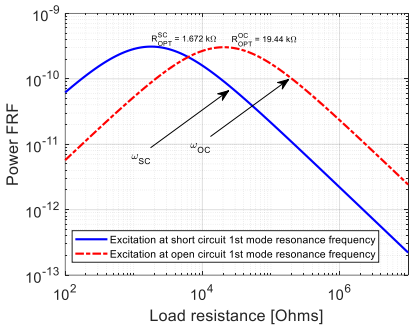

(b)

Figure 11. Voltage and power outputsversus a broad range of load resistance at the short and open circuits of the 1st vibrational mode.

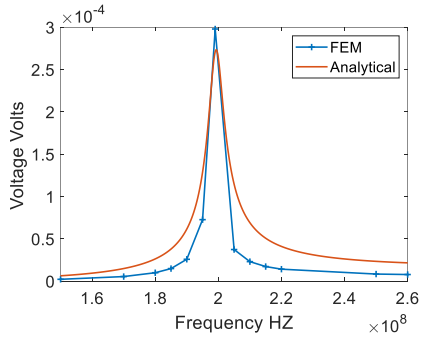

(a)

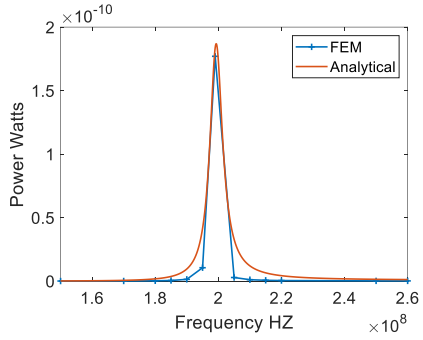

(b)

Figure 12. Analytically and numerically obtained (a) voltage and (b) power outputsversus a broad rangeof base excitation.

5.3. Simulation of the Optimized Device

This section shows the simulation of the optimized device with the optimal dimensions over a wide range of frequencies. FEM COMSOL is used to simulate the device in the frequency domain and to evaluate the voltage and output power. The output power utilized in simulation can be expressed as follows[60]:

$$Power = \left(\frac{R\,\alpha_2{}^2}{\left(\frac{\pi}{2}+Rc_p\omega_n\right)^2}\frac{\omega_n{}^4\,U^2M^2}{\left(C_v+\left(2R\,\alpha_2{}^2/\left(Rc_p\omega_n+\left(\frac{\pi}{2}\right)^2\right)\right)\right)^2}\right) \quad (12)$$

The power output can also be expressed as:

$$Power = V_{re}\left(\frac{2\alpha_2}{\frac{\pi}{2}+Rc_p\omega_n}+C_v\frac{\frac{\pi}{2}+Rc_p\omega_n}{\alpha_2 R}\right) \quad (13)$$

Where, α_2 represents the electromechanical coupling coefficient of PZT materials, $V_{re}$is the rectified voltage,c_p is the capacitance,C_V is the damping coefficient (N/ms),M is the dynamic mass,U is the base excitation (in meters),U is the base excitation (m/s^2),ω_n is the natural frequency, and$R$ is the electrical load resistance.

The iterative optimization utilized in the previous section is implemented by changing the thickness of piezoelectric and copper layers to reach the targeted frequency. The dimensions of the copper layer are (10x10^{-4} mm by 5x10^{-4} mmby 1.85 x10^{-4} mm). The physical dimensions of the PZT layer are (10x10^{-4} mm by 5x10^{-4} mmby 2.25 x10^{-4}mm).

At this point, many optimization attempts using the three optimization algorithms are conducted. The results of optimization are revealed in the previous section. The simulation of the optimal dimensions resulted from this optimization is conducted using FEM. Figure 13 reveals the power and voltage against a broad range of the electric resistance of the optimized device using three optimization algorithms. Figure 14 shows the response of the voltage of the optimized device in frequency domain. Figure 15 reveals the power frequency response of the optimized device. From the results of the previous figures, it is founded that the optimal resistance, voltage, and powerare3.2 Ω,1.22x10^{-3}, volts, and2.4 x10^{-4}mW, respectively.

The results of BOBYQA optimization algorithm obviously outweigh the other optimization algorithms including the iterative optimization method. Table 6 compared the results between the iterative and BOBQYA optimization algorithms. The voltage and power required to operate a typical 5 mm LED indicator are 3.4 V and 0.0022 mW, respectively. The voltage and power generated by the proposed sensing device are not enough to power the LED indicator. Therefore, an amplifier is needed. The amplifier and the LED setup can be easily established as in the literature.

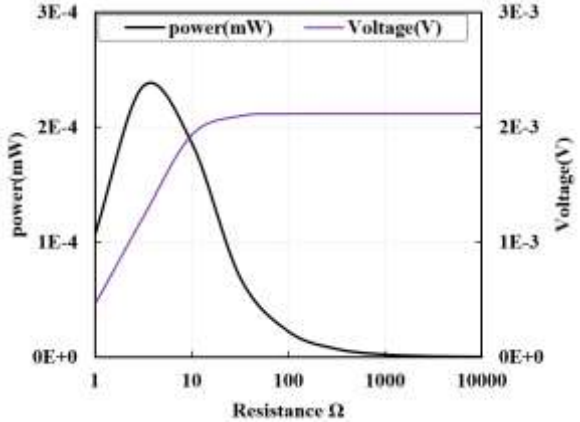

Figure 13. The power and voltage Vs electric resistance of the optimized sensing device using three optimization algorithms.

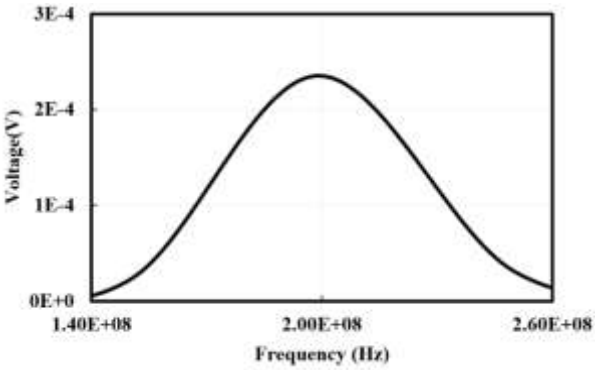

Figure 14. The frequency response of the voltage of the optimized sensing device.

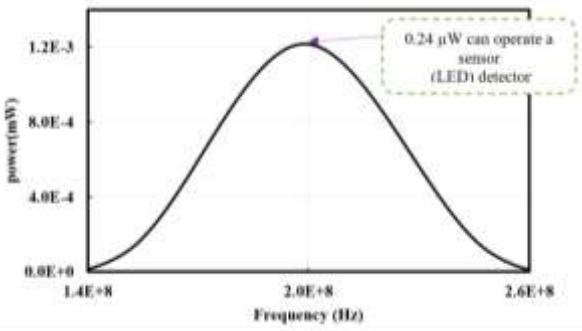

Figure 15. The frequency response of the power of the optimized sensing device.

Table 6. The comparison between iterative and BOBQYA optimization algorithm results.

Harvester parameters	Un-optimized	BOBYQA optimization algorithm
(L mm)	10 x10^{-4}	10 x10^{-4}
(wmm)	5 x10^{-4}	5.3 x10^{-4}
(t_p mm)	1.85 x10^{-4}	1 x10^{-4}
($t_s$mm)	2.25 x10^{-4}	2.99 x10^{-4}
Voltage (V)	3.8 x10^{-4}	1.22 x10^{-4}
Power (mW)	7.01 x10^{-4}	2.4 x10^{-4}

We conclude this section by showing a brief comparison table that compares past studies to this current work. The comparison is illustrated in Table 7that reveals that the proposed optimized device outperforms other techniques found in the literature. The power density of the proposed device outweighs the similar devices found in literature due to the optimization technique used in this paper as manifested in the volume dimensions and the corresponding natural frequencies.

Table 7. Performance comparison of the proposed device with other techniques in the literature.

Ref.	Excitation; g = 9.8 m s^{-2}	Frequency range (Hz)	Piezo Size (mm^3)	Mass (g)	Power	Power Density (mWmm^{-3})
This study	3.5 x10^{-12}g	5-22	2.1 x10^{-10}	~0	0.24 µW	1.14e6
[61]	0.5g	56	5918.9	100	4.76 µW	0.804e-6
[62]	0.25g	68	0.11	5	0.023 µW	0.209e-3
[63]	3.5g	75	56	7.8	0.239 µW	4.27e-6

It must be mentioned that MEMS sensors output responses can be affected by environmental conditions, such as temperature, humidity, vibration, and electromagnetic interference. Our proposed sensor device can be sensitive to temperature changes, and the output responses can drift or change with temperature fluctuations resulting in changes in the output voltage[64]. Furthermore, humidity can affect the performance of our proposed sensor that measure acceleration[65]. In addition, unwanted vibration from the

environment can cause mechanical stress to our proposed sensor structures, leading to changes in the sensor's output responses[66].

Our proposed sensor measures acceleration and its precise mechanical movement can be interfered by Electromagnetic Interference (EMI) sources such as mobile phones, Wi-Fi, or other electronic devices and can induce noise in the sensor output, leading to errors in the reading. All these effects should be considered in future experiment work and compensation techniques may need to be applied such as calibration or signal processing algorithms to mitigate the effects of environmental conditions on the sensor output.

6. Potentiality Treatment of COVID-19

Although the spike proteins of COVID-19 are different in structures, they have close natural frequencies. The frequency variations are in the range of 1.99 $x10^8$Hz to 2.09 $x10^8$ Hz. The essential purpose of this paper is to detect the virus by powering a LED. The output voltage must be amplified since the power generated wasn't enough to power a typical LED. The motion of the spike can be considered as excitation input to the proposed piezoelectric device. Furthermore, once the infection is detected, the virus can be eliminated through an ultrasonic resonance device. The strength of the spike protein is unspecified. Therefore, it is assumed that its value is lower than 300 MPa. Therefore, the failure of the spike protein introduces by the resonance effect or the stresses of the ultrasonic device is greater than 300 MPa. The necessary damage excitation acceleration and amplitude are evaluated to be 4.164 m/s^2 and 1.041 $x10^5$mm, respectively, and are in the safe range to the human body [67]. This investigation was conducted by Randall et al. [68],where the typical human frequencies were determined to be between 9 and 16 Hz. Therefore, the ultrasonic device will not cause any harm to the patient since the human body's frequencies are not in the resonance range of the sensing device operating frequency.

7. Conclusions

This paper introduced a discussion about installing the micro scale piezoelectric energy device in a human body. An optimized piezoelectric sensing device with same frequency of COVID-19 was introduced. Modeling a piezoelectric energy device with frequency equals to the COVID-19 natural frequency was presented. The Eigen frequency study was employed to optimize the natural frequency of the sensing device iteratively. Then an optimization method for the proposed sensing device was conducted using three different optimization algorithms. The optimal electric resistance was 10KΩ using the iterative optimization technique. The optimal electric resistance was 3.2 Ω in BOBYQA optimization algorithm. The frequency response of the voltage and power were presented. The optimal voltage and power were 4.5 $x10^{-3}$V and 7.01$x10^{-7}$mW, respectively using the iterative optimization. Algorithm. Using BOBYQA optimization algorithm, the optimal voltage and power were 1.22 $x10^{-3}$ V and 2.4 $x10^{-4}$mW, respectively. An external amplifier must be used to amplify the electrical power generated by the piezoelectric layer of the proposed sensor since the power generated wasn't enough to power a typical LED. Therefore, it is recommended to explore other configurations of the proposed sensing device in future work with different scenarios to detect a possible COVID-19 infection. An ultrasonic device could be used to eliminate the COVID-19 virus to speed up the healing a recovery process. The analytical model was presented using Euler–Bernoulli theory. The voltage and power frequency response for open and closed circuits were simulated analytically against a wide range of excitation frequencies. The analytical results were employed to verify the Finite Element Method (FEM) that found in a very good agreement. It can be concluded that all available COVID-19 tests are invasive and expensive such as Polymerase chain reaction test (PCR). Therefore, it was vital to explore noninvasive procedures to detect and eliminate this pandemic expeditious. The benefits of this study was introducing a rapid, efficient and affordable technique to detect and quarantine the SARS-COVID-19 by designing a piezoelectric sensing device that resonated with the virus's natural frequency so that an ultrasonic resonance device could be used to eliminate the virus. Our proposed technique was both fast and inexpensive compared to conventional tests.

References

[1] M. Yao and H. Wang, "A potential treatment for COVID-19 based on modal characteristics and dynamic responses analysis of 2019-nCoV," Nonlinear dynamics, vol. 106, no. 2, pp. 1425-1432, 2021.

[2] World Health Organization. WHO statement regarding cluster of pneumonia cases in Wuhan, China. https://www. who.int/china/news/detail/09-01-2020-who-statementregarding-cluster-of-pneumonia-cases-in-wuhan- china. Accessed 25 Apr 2020.

[3] National Health Commission of the People's Republic of China. Interim protocol of diagnosis and treatment of 2019 novel coronavirus-associated pneumonia (the second ver- sion). http://www.nhc.gov.cn/jkj/s3577/202001/c67cfe29 ecf1470e8c7fc47db751e88.shtml. Accessed 25 Apr 2020.

[4] N. Zhu et al., "A novel coronavirus from patients with pneumonia in China, 2019," New England journal of medicine, 2020.

[5] W. H. Organization, "Novel Coronavirus (2019-nCoV): situation report, 11," 2020.

[6] W. H. O. 22/9/2021.

[7] C. Williams and R. B. Yates, "Analysis of a micro-electric generator for microsystems," sensors and actuators A: Physical, vol. 52, no. 1-3, pp. 8-11, 1996.

[8] I. M. Aladwan, C. Bazilo, and E. Faure, "Modelling and Development of Multisectional Disk Piezoelectric Transducers for Critical Application Systems," Jordan Journal of Mechanical & Industrial Engineering, vol. 16, no. 2, 2022.

[9] E. J. Majeed and A. J. Majeed, "Harvesting Human Being Energy to Charge Smartphone," Jordan Journal of Mechanical & Industrial Engineering, vol. 16, no. 3, 2022.

[10] O. Mokhiamar, D. O. Masara, and H. El Gamal, "Performance Enhancement of Multi-Modal Piezoelectric Energy Harvesting Through Parameter Optimization," Jordan Journal of Mechanical & Industrial Engineering, vol. 16, no. 5, 2022.

[11] J. Lange, J. Hilgedieck, and M. Kaltschmitt, "Renewable Resources of Energy for Electricity Generation-Development Trends and Necessities Within the Overall Energy System," Jordan Journal of Mechanical & Industrial Engineering, vol. 13, no. 3, 2019.

[12] S. H. H. Kachapi, "Nonlinear Vibration and Frequency Analysis of Functionally Graded-Piezoelectric Cylindrical Nano-shell with Surface Elasticity," Jordan Journal of Mechanical & Industrial Engineering, vol. 12, no. 4, 2018.

[13] F. Ebrahimi and M. R. Barati, "Buckling Analysis of Nonlocal Embedded Shear Deformable Functionally Graded Piezoelectric Nanoscale Beams," Jordan Journal of Mechanical & Industrial Engineering, vol. 11, no. 2, 2017.

[14] K. Mohamed, H. Elgamal, and S. A. Kouritem, "An experimental validation of a new shape optimization technique for piezoelectric harvesting cantilever beams," Alexandria Engineering Journal, vol. 60, no. 1, pp. 1751-1766, 2021/02/01/ 2021, doi: https://doi.org/10.1016/j.aej.2020.11.024.

[15] S. Fang et al., "Broadband energy harvester for low-frequency rotations utilizing centrifugal softening piezoelectric beam array," Energy, vol. 241, p. 122833, 2022.
[16] Y. Jian, L. Tang, G. Hu, Z. Li, and K. C. Aw, "Design of graded piezoelectric metamaterial beam with spatial variation of electrodes," International Journal of Mechanical Sciences, vol. 218, p. 107068, 2022.
[17] Z. Wang, Y. Du, T. Li, Z. Yan, and T. Tan, "A flute-inspired broadband piezoelectric vibration energy harvesting device with mechanical intelligent design," Applied Energy, vol. 303, p. 117577, 2021.
[18] M. Li and X. Jing, "Novel tunable broadband piezoelectric harvesters for ultralow-frequency bridge vibration energy harvesting," Applied Energy, vol. 255, p. 113829, 2019.
[19] L. Staaf, A. Smith, P. Lundgren, P. Folkow, and P. Enoksson, "Effective piezoelectric energy harvesting with bandwidth enhancement by assymetry augmented self-tuning of conjoined cantilevers," International Journal of Mechanical Sciences, vol. 150, pp. 1-11, 2019.
[20] X. Rui et al., "Design and experimental investigation of a self-tuning piezoelectric energy harvesting system for intelligent vehicle wheels," IEEE Transactions on Vehicular Technology, vol. 69, no. 2, pp. 1440-1451, 2019.
[21] H. Kim, W. C. Tai, J. Parker, and L. Zuo, "Self-tuning stochastic resonance energy harvesting for rotating systems under modulated noise and its application to smart tires," Mechanical Systems and Signal Processing, vol. 122, pp. 769-785, 2019.
[22] S. A. Kouritem, "Array of piezoelectric energy harvesters for broadband natural frequency applications," in Proceedings of the ICSV27, Annual Congress of International Institute of Acoustics and Vibration (IIAV), Prague, Czech Republic, 2021, pp. 11-16.
[23] D. O. Masara, H. El Gamal, and O. Mokhiamar, "Split cantilever multi-resonant piezoelectric energy harvester for low-frequency application," Energies, vol. 14, no. 16, p. 5077, 2021.
[24] A. R. G. da Silveira and G. B. Daniel, "Optimization analysis of an energy harvester for smart tilting pad journal bearings considering higher vibration modes," Mechanical Systems and Signal Processing, vol. 166, p. 108404, 2022.
[25] C. Liu, B. Liao, R. Zhao, K. Yu, H. P. Lee, and J. Zhao, "Large stroke tri-stable vibration energy harvester: Modelling and experimental validation," Mechanical Systems and Signal Processing, vol. 168, p. 108699, 2022.
[26] M. Bani-Hani, V. Krovi, and M. A. Karami, "Modeling of a beam with a mass in the middle for heart beat vibration energy harvesting," in International Design Engineering Technical Conferences and Computers and Information in Engineering Conference, 2014, vol. 46414: American Society of Mechanical Engineers, p. V008T11A092.
[27] S. C. Bonawitz, "Management of exposure of cardiac pacemaker systems," Annals of plastic surgery, vol. 69, no. 3, pp. 292-295, 2012.
[28] K. Burney, F. Burchard, M. Papouchado, and P. Wilde, "Cardiac pacing systems and implantable cardiac defibrillators (ICDs): a radiological perspective of equipment, anatomy and complications," Clinical radiology, vol. 59, no. 8, pp. 699-708, 2004.
[29] A. Cheng and L. G. Tereshchenko, "Evolutionary innovations in cardiac pacing," Journal of Electrocardiology, vol. 44, no. 6, pp. 611-615, 2011.
[30] G.-T. Hwang et al., "In vivo silicon-based flexible radio frequency integrated circuits monolithically encapsulated with biocompatible liquid crystal polymers," Acs Nano, vol. 7, no. 5, pp. 4545-4553, 2013.
[31] S. J. Majerus, S. L. Garverick, M. A. Suster, P. C. Fletter, and M. S. Damaser, "Wireless, ultra-low-power implantable sensor for chronic bladder pressure monitoring," ACM Journal on Emerging Technologies in Computing Systems (JETC), vol. 8, no. 2, pp. 1-13, 2012.
[32] H. G. Mond, J. G. Sloman, and R. H. Edwards, "The first pacemaker," Pacing and Clinical Electrophysiology, vol. 5, no. 2, pp. 278-282, 1982.
[33] S. Pezet and S. B. McMahon, "Neurotrophins: mediators and modulators of pain," Annu. Rev. Neurosci., vol. 29, pp. 507-538, 2006.
[34] E. Jiatong, L. Lanquin, and L. Wenjun, "Epidemia de COVID-19: características de la enfermedad en niños," Journal of Medical Virology, vol. 92, pp. 747-754, 2020.
[35] B. Vellingiri et al., "COVID-19: A promising cure for the global panic," Science of the total environment, vol. 725, p. 138277, 2020.
[36] H. Shi et al., "Radiological findings from 81 patients with COVID-19 pneumonia in Wuhan, China: a descriptive study," The Lancet infectious diseases, vol. 20, no. 4, pp. 425-434, 2020.
[37] L.-F. Wang and D. E. Anderson, "Viruses in bats and potential spillover to animals and humans," Current opinion in virology, vol. 34, pp. 79-89, 2019.
[38] X. Wang, S. Stelzer-Braid, M. Scotch, and W. D. Rawlinson, "Detection of respiratory viruses directly from clinical samples using next-generation sequencing: A literature review of recent advances and potential for routine clinical use," Reviews in Medical Virology, vol. 32, no. 5, p. e2375, 2022.
[39] F. Ali, W. Raza, X. Li, H. Gul, and K.-H. Kim, "Piezoelectric energy harvesters for biomedical applications," Nano Energy, vol. 57, pp. 879-902, 2019.
[40] Y. M. Bar-On, A. Flamholz, R. Phillips, and R. Milo, "SARS-CoV-2 (COVID-19) by the numbers," elife, vol. 9, p. e57309, 2020.
[41] J. Y. Cho et al., "A multifunctional road-compatible piezoelectric energy harvester for autonomous driver-assist LED indicators with a self-monitoring system," Applied Energy, vol. 242, pp. 294-301, 2019.
[42] Y. Hong, L. Sui, M. Zhang, and G. Shi, "Theoretical analysis and experimental study of the effect of the neutral plane of a composite piezoelectric cantilever," Energy conversion and management, vol. 171, pp. 1020-1029, 2018.
[43] M. S. Abdeljaber, "Nonlinear Natural Frequencies and Frequency Veering of a Beam with an Arbitrary Initial Rise Supported by Flexible Ends and Resting on Elastic Foundation," JJMIE, vol. 11, no. 3, 2017.
[44] M. A. Gharaibeh, A. A. Ismail, A. F. Al-Shammary, and O. A. Ali, "Three-Material Beam: Experimental Setup and Theoretical Calculations," Jordan Journal of Mechanical & Industrial Engineering, vol. 13, no. 4, 2019.
[45] A. Erturk and D. J. Inman, "A distributed parameter electromechanical model for cantilevered piezoelectric energy harvesters," Journal of vibration and acoustics, vol. 130, no. 4, 2008.
[46] A. Meitzler, D. Berlincourt, F. Welsh III, H. Tiersten, G. Coquin, and A. Warner, "IEEE Standard on PiezoelectricityIEEE," New York, 1988.
[47] M. A. Bani-Hani, A. M. Almomani, K. F. Aljanaideh, and S. A. Kouritem, "Mechanical Modeling and Numerical Investigation of Earthquake-Induced Structural Vibration Self-Powered Sensing Device," IEEE Sensors Journal, vol. 22, no. 20, pp. 19237-19248, 2022.
[48] G. K. Ottman, H. F. Hofmann, A. C. Bhatt, and G. A. Lesieutre, "Adaptive piezoelectric energy harvesting circuit for wireless remote power supply," IEEE Transactions on power electronics, vol. 17, no. 5, pp. 669-676, 2002.
[49] M. Guan and W. Liao, "On the efficiencies of piezoelectric energy harvesting circuits towards storage device voltages," Smart Materials and Structures, vol. 16, no. 2, p. 498, 2007.
[50] A. Erturk and D. J. Inman, Piezoelectric energy harvesting. John Wiley & Sons, 2011.
[51] F. Goldschmidtboeing and P. Woias, "Characterization of different beam shapes for piezoelectric energy harvesting," Journal of Micromechanics and Microengineering, vol. 18, no. 10, p. 104013, 2008/09/29 2008, doi: 10.1088/0960-1317/18/10/104013.
[52] O. Abuzeid, A. Daoud, and M. Barghash, "Optimal Off-Grid Hybrid Renewable Energy System for Residential Applications Using Particle Swarm Optimization," Jordan Journal of Mechanical & Industrial Engineering, vol. 13, no. 2, 2019.

[53] M. Rahimi and H. Fazlollahtabar, "Optimization of a Closed Loop Green Supply Chain using Particle Swarm and Genetic Algorithms," Jordan Journal of Mechanical & Industrial Engineering, vol. 12, no. 2, 2018.

[54] A. Benatiallah, L. Kadia, and B. Dakyob, "Modelling and optimisation of wind energy systems," JJMIE, vol. 4, no. 1, 2010.

[55] N. Khodadadi and S. Mirjalili, "Truss optimization with natural frequency constraints using generalized normal distribution optimization," Applied Intelligence, 2022/01/13 2022, doi: 10.1007/s10489-021-03051-5.

[56] S. A. Kouritem and M. M.Y.B. Elshabasy, "Tailoring the panel inertial and elastic forces for the flutter and stability characteristics enhancement using copper patches," Composite Structures, vol. 274, p. 114311, 2021/10/15/ 2021, doi: https://doi.org/10.1016/j.compstruct.2021.114311.

[57] M. M.Y.B. Elshabasy and S. A. Kouritem, "Thickening of optimally selected locations on panels subjected to unyawed flow for substantial delay of the panel flutter," Alexandria Engineering Journal, vol. 59, no. 6, pp. 5031-5044, 2020/12/01/ 2020, doi: https://doi.org/10.1016/j.aej.2020.09.026.

[58] M. J. D. Powell, "The BOBYQA algorithm for bound constrained optimization without derivatives," 2009.

[59] M. J. D. Powell, "A View of Algorithms for Optimization without Derivatives," Technical Report DAMTP2007/NA03, Department of Applied Mathematics and Theoretical Physics, University of Cambridge, Cambridge, 2007.

[60] E. Lefeuvre, D. Audigier, C. Richard, and D. Guyomar, "Buck-Boost Converter for Sensorless Power Optimization of Piezoelectric Energy Harvester," IEEE Transactions on Power Electronics, vol. 22, no. 5, pp. 2018-2025, 2007, doi: 10.1109/TPEL.2007.904230.

[61] J. Wu, X. Chen, Z. Chu, W. Shi, Y. Yu, and S. Dong, "A barbell-shaped high-temperature piezoelectric vibration energy harvester based on BiScO3-PbTiO3 ceramic," Applied Physics Letters, vol. 109, no. 17, p. 173901, 2016.

[62] C.-F. Hung, T.-K. Chung, P.-C. Yeh, C.-C. Chen, C.-M. Wang, and S.-H. Lin, "A miniature mechanical-piezoelectric-configured three-axis vibrational energy harvester," IEEE Sensors Journal, vol. 15, no. 10, pp. 5601-5615, 2015.

[63] H.-C. Song et al., "Ultra-low resonant piezoelectric MEMS energy harvester with high power density," Journal of Microelectromechanical Systems, vol. 26, no. 6, pp. 1226-1234, 2017.

[64] D. Strle and V. Kempe, "MEMS-based inertial systems," INFORMACIJE MIDEM-LJUBLJANA-, vol. 37, no. 4, p. 199, 2007.

[65] M. T. Jan, F. Ahmad, N. H. B. Hamid, M. H. B. M. Khir, M. Shoaib, and K. Ashraf, "Experimental investigation of temperature and relative humidity effects on resonance frequency and quality factor of CMOS-MEMS paddle resonator," Microelectronics Reliability, vol. 63, pp. 82-89, 2016.

[66] C. Patel and P. McCluskey, "Performance of MEMS Vibratory Gyroscope under Harsh Environments," Additional Papers and Presentations, vol. 2012, no. DPC, pp. 000633-000654, 2012.

[67] D. H. Glaister, "Human tolerance to impact acceleration," Injury, vol. 9, no. 3, pp. 191-198, 1978.

[68] J. Randall, R. Matthews, and M. Stiles, "Resonant frequencies of standing humans," Ergonomics, vol. 40, no. 9, pp. 879-886, 1997.